Renewable Energy and Power Quality Journal
https://repqj.com/index.php/repqj/index
RE&PQJ, Vol. 24, No. 4, 2026

Comparative Study of Metaheuristic Algorithms Applied to PI and FOPI Controllers for DFIG-Based Wind Turbine Systems

Omar Abdelaziz Bengharbi[1,*], Karim Beddek[1], Rezki Haddouche[2], Karim Benalia[3]

[1]Department of Automation and Electrification, Laboratory of Applied Automation, University of Boumerdes M'Hamed Bougara, Faculty of Hydrocarbons and Chemistry, Boumerdes, Algeria

[2]Department of Power and Control, Institute of Electrical and Electronic Engineering, University of Boumerdes, Algeria

[3]Department of Mathematical Sciences, Faculty of Hydrocarbons and Chemistry, Laboratory of Operational Research, Boumerdes, Algeria

[*]Corresponding Author: Omar Abdelaziz Bengharbi, o.bengharbi@univ-boumerdes.dz

Article History

Received: 09 May 2026 Revised: 11 July 2026 Accepted: 14 July 2026 Available Online: 05 August 2026

Abstract. With the objective of improving dynamic response and enhancing power extraction, this work proposes a metaheuristic-based design of a Fractional-Order Proportional-Integral (FOPI) regulator for a Doubly-Fed Induction Generator (DFIG). A two-stage offline tuning strategy based on four metaheuristic algorithms, namely Grey Wolf Optimization (GWO), Equilibrium Optimizer (EO), Particle Swarm Optimization (PSO), and Harris Hawk Optimization (HHO), was employed to optimize the FOPI parameters. The algorithms were comparatively evaluated, and GWO emerged as the best-performing optimization technique. Subsequently, a comparative analysis between the conventional PI and the optimized FOPI controllers were conducted, focusing on dynamic response. The results demonstrated the superior performance of the FOPI controller across multiple performance indicators, with improvements ranging from 2% to 40% in overshoot, settling time, and steady-state error. These enhancements were further supported by the Integral Absolute Error (IAE) metric, where the FOPI controller yields lower errors for I_d (2.9978 versus 3.0237), I_q (1.5456 versus 2.6367), and V_{dc} (4.0076 versus 6.7130). In addition, the optimized FOPI controller improved the reactive power behaviour by reducing rotor-side oscillations and achieved a 17% reduction in stator-side reactive power. These findings validate the effectiveness of the proposed two-stage optimized FOPI control strategy in improving dynamic response, reducing control errors, and enhancing the overall stability and performance of DFIG-based wind energy conversion systems

Key words. Fractional-order PID, Grey wolf optimization, Wind turbine system, Doubly fed Induction generator, Metaheuristic algorithms.

1. Introduction

The global transition toward green and sustainable energy has accelerated significantly in recent years due to growing concerns about climate change and the increasing demand for clean electricity. Consequently, renewable energy systems, particularly Photovoltaic (PV) and Wind Energy Conversion Systems (WECSs), have attracted considerable attention from both academia and industry [1]. Alongside this transition, there is a continuous need to improve system efficiency while reducing operational and implementation costs. Although substantial technological advancements have been achieved, modern energy systems have become increasingly complex, creating a challenging trade-off between simplicity and performance.

The core complexity of these systems is the control strategy adopted. Among the available control strategies, the Fractional-Order Proportional–Integral–Derivative (FOPID) controller has emerged as an attractive solution owing to its simple structure and enhanced flexibility compared with PID controller. However, determining the optimal FOPID parameters remains a challenging task because of the additional fractional orders and the nonlinear characteristics of many practical systems [2]. To address this issue, numerous metaheuristic optimization algorithms have been proposed and successfully applied to controller tuning problems across various engineering domains. These optimization-based tuning approaches have gained particular importance in WECS applications in recent years [3].

Since modern wind power systems commonly employ induction machines, the Doubly Fed Induction Generator (DFIG) has become one of the most widely investigated technologies in wind energy conversion systems. Unlike fixed-speed induction generators, such as the Squirrel Cage Induction Generator (SCIG), the DFIG offers variable-speed operation, enabling more efficient wind energy extraction and improved system performance [4,5].

The DFIG architecture employs a pair of converters, the Grid-Side Converter (GSC) and the Rotor-Side Converter (RSC), which work in tandem to generate electricity efficiently. The GSC ensures a consistent DC-link voltage that serves as the RSC's voltage source, and the RSC controls the active and reactive power output by modulating the magnetization currents in the rotor windings, enabling precise regulation of the stator's power delivery [5,6]. Furthermore, the GSC is versatile in that it can compensate for reactive power and manage unstable conditions, such as the removal of reactive power pulses. The complex cooperation of these converters, each with unique features, underscores the importance of carefully selecting control parameters for optimizing the performance [5].

In the last few decades, a variety of control techniques, including both conventional and stochastic models, have made significant advancements in contemporary industry. The most popular of these is the Proportional Integral-Derivative (PID) regulator, which is recognised as a reliable, simple-structured controller capable of adapting to various operating circumstances [7]. Because PID controllers are easy to install, they are widely used; however, their limitations sometimes pose difficulties when dealing with complex dynamics in industry [8]. Thus, researchers have been developing alternatives to address these limitations.

In consideration of WECS, [9] tackled the issue of Sub-Synchronous Interactions (SSI) in grid-connected DFIG wind turbines. Leveraging an optimization model driven by non-dominated sorting genetic algorithms and t-distributed stochastic neighbour embedding, this study explored optimal PI parameter ranges for oscillation restraint and damping augmentation. Simulation and practical experimentation underscored the efficacy of this approach in quelling SSI, offering promise for power system stability while integrating wind power. Expanding on these advancements, [10] Prakash et al. employed Bacterial Foraging Optimization (BFO) and Particle Swarm Optimization (PSO) algorithms to optimize the DFIG control system, furnishing invaluable insights and a simulation-based performance analysis as a basis for future advancements. With the same algorithms used in the previous work, Bakir et al. [5] provided simulation results and validated them with experiments. Similarly, a metaheuristics-based design leveraging the Thermal Exchange Optimization (TEO) algorithm for tuning PI controllers in direct power control schemes, backed by statistical analyses showcasing its competitive performance in tackling global optimization problems, was presented in [6].

In parallel with optimization-based tuning techniques, intelligent control strategies have attracted considerable attention for improving the performance of systems under varying operating conditions. In this context, fuzzy logic has been widely integrated with conventional controllers to enhance adaptability and robustness. A fuzzy logic self-adaptive PI controller was proposed in [11], where comparative analyses with conventional PI and fuzzy logic controllers demonstrated improved reduction of steady-state errors, current fluctuations, and total harmonic distortion, while maintaining satisfactory dynamic performance under parameter uncertainties and random wind variations. Similarly, a hybrid PID-Fuzzy Logic controller was investigated for grid-connected DFIG systems in [12], exhibiting superior tracking accuracy, stability, and robustness compared with conventional PI-based control structures. Moreover, advanced control techniques such as Finite-Control-Set Model Predictive Control (FCS-MPC) were explored. In [13], a comparative study between FCS-MPC and a fuzzy self-adaptive PI controller revealed that predictive control provided enhanced accuracy, robustness, and reduced power fluctuations over a wide range of operating conditions. These developments highlight the ongoing efforts to improve the dynamic performance and robustness of DFIG control systems through the integration of intelligent and advanced control methodologies.

Despite the widespread use and reliability of PID controllers, their effectiveness can be limited when dealing with complex dynamics [8]. In such scenarios, researchers have sought to augment control methodologies to overcome these limitations and achieve superior performance. One notable advancement in this regard, presented by Podlubny, is the FOPID controller [14]. By integrating principles of fractional calculus into the traditional PID framework, FOPID controllers offer enhanced adaptability and precision, making them a well suited alternative for modern industrial processes. This innovation led to active exploration of FOPID control strategies across various systems.

Within this framework, Asgharnia et al. [15] introduced optimal fuzzy PID and fractional-order fuzzy PID controllers for controlling wind turbine pitch angles above rated wind speed, employing PSO and Differential Evolution (DE) to achieve optimal parameterization. The fractional-order fuzzy PID controller particularly showed strong performance in minimizing error and control effort while addressing inherent uncertainties in wind turbine dynamics. Additionally, Li et al. [16] proposed a fractional-order sliding mode control strategy to mitigate sub-synchronous control interaction in wind farms, using feedback linearization and genetic algorithm-based parameter tuning to ensure robust stabilization under disturbances and parameter variations. Furthermore, Yang et al. [17] developed an adaptive FOPID control scheme based on linear observers for perturbation estimation, combined with adaptive mechanisms to enhance robustness and power extraction efficiency in wind turbines. In [18], an FOPI controller integrated with a neuro-fuzzy PWM technique was applied to multi-rotor wind turbine systems. Other studies reported theoretical work and improved system performance in various applications [19-22], including different WECS configurations [23-25].

Other work has further investigated metaheuristic and intelligent optimization techniques for fractional-order controller design. In particular, optimization-based methods such as Ebola optimization search combined with spiking neural networks (EOSA-SNN) [26], Grey Wolf Optimization (GWO) [27], and Remora Optimization Algorithm (ROA) [28] were applied to FOPID/FOPI structures, demonstrating improved active and reactive power regulation, reduced total harmonic distortion, and enhanced dynamic response under variable wind conditions. In addition, Particle Swarm Optimization (PSO)-based fractional-order PI/FOPI controllers were successfully implemented in grid-connected renewable energy systems, achieving improved robustness, stability, and power quality compared to conventional PI controllers [29]. Moreover, modified control strategies such as fractional-order-based direct power control applied to multi-rotor wind turbine systems [30] have reported significant reductions in power ripple, steady-state error, and current harmonics. Finally, the comparative study by Bingul and Karahan [31] evaluated PID and FOPID controllers optimized using PSO and Artificial Bee Colony (ABC) algorithms, providing useful insights into dynamic response and robustness under disturbances in wind turbine control systems.

Despite the progress made in the development of control techniques for WECS, further research is essential to establish a simple yet performant controller. The FOPI controller introduces additional degrees of freedom, offering improved flexibility and the potential to optimize system dynamics. However, tuning such controllers is challenging due to the high-dimensional and complex nature of the system, where achieving stability, maximizing power extraction, and maintaining simplicity and efficiency are the objectives.

Motivated by these considerations, the main objective of this work is to design and optimize a FOPI controller for a DFIG-based wind energy conversion system and to evaluate its performance. The principal contributions of this study are summarized as follows:

- Development of a two-stage optimization strategy for tuning both the proportional-integral gains and the fractional-order parameters of the FOPI controller.
- Comparative evaluation of four metaheuristic optimization algorithms: Grey Wolf Optimization (GWO), Particle Swarm Optimization (PSO), Equilibrium Optimizer (EO), and Harris Hawk Optimization (HHO), for controller parameter tuning.
- Comprehensive performance assessment of optimized PI and FOPI controllers based on dynamic response.
- Demonstration that the optimized FOPI controller improves reactive power regulation by reducing oscillations and enhancing stabilization in both the stator and rotor sides, thereby contributing to improved overall system stability.

In this work, a modeling of the DFIG system adopting the Direct-Quadrature (d-q) rotating reference frame is first presented, providing a foundational understanding of the system's dynamic behaviour. Following this, the theory of FOPID controllers is explored, and the relevant literature is reviewed. Building upon that foundation, a feedback control system for the DFIG is designed, and the minimization problem is formulated to be addressed using advanced metaheuristic algorithms. Finally, the results are analysed and discussed, with an evaluation of the performance improvements offered by the proposed control strategy.

2. DFIG Modelling

The DFIG is appropriate for a wide range of applications because of its exceptional dependability and endurance. However, its complex equation system for analysis and control is challenging. We address this complexity by using the Park transformation and simplifying assumptions to derive a more straightforward model. The generator voltage equations, assuming that the d-q-axis spins at the synchronous speed [32,33]:

$$\begin{cases} v_{ds}=\dfrac{d\Psi_{ds}}{dt}+R_s i_{ds}-\omega_s\Psi_{qs} \\ v_{qs}=\dfrac{d\Psi_{qs}}{dt}+R_s i_{qs}+\omega_s\Psi_{ds} \\ v_{dr}=\dfrac{d\Psi_{dr}}{dt}+R_r i_{dr}-s\omega_s\Psi_{qr} \\ v_{qr}=\dfrac{d\Psi_{qr}}{dt}+R_r i_{qr}+s\omega_s\Psi_{dr} \end{cases} \tag{1}$$

The stator and rotor magnetic flux equations are given by:

$$\begin{cases} \Psi_{ds}=i_{dr}L_m+i_{ds}L_s \\ \Psi_{qs}=i_{qr}L_m+i_{qs}L_s \\ \Psi_{dr}=i_{ds}L_m+i_{dr}L_r \\ \Psi_{qr}=i_{qs}L_m+i_{qr}L_r \end{cases} \tag{2}$$

Where the stator and rotor voltages and currents (in dq-axis) are represented by v_{qs}, v_{ds}, i_{qs}, i_{ds}, v_{qr}, v_{dr}, i_{qr}, and i_{dr} .

ω_s is the synchronous reference frame's rotational speed; s is the slip; $s\omega_s=(\omega_s-\omega_e)$ is the slip frequency, and ω_e is the generator electrical speed. L_m is the mutual inductance, R_s, R_r and L_s, L_r are the stator and rotor resistances and inductances.

The active and reactive stator and rotor powers are given by:

$$\begin{cases} P_s=\dfrac{3}{2}\left(v_{qs}i_{qs}+v_{ds}i_{ds}\right) \\ Q_s=\dfrac{3}{2}\left(v_{ds}i_{qs}-v_{qs}i_{ds}\right) \\ P_r=\dfrac{3}{2}\left(v_{qr}i_{qr}+v_{dr}i_{dr}\right) \\ Q_r=\dfrac{3}{2}\left(v_{dr}i_{qr}-v_{qr}i_{dr}\right) \end{cases} \tag{3}$$

Where the power losses due to the rotor and stator resistances are disregarded.

3. Fractional Order Calculus & FOPID

In mathematics, Fractional Order Calculus (FOC) is an area that deals with differentiation and integration with a real integer. The differintegral operator, abbreviated ${}_aD_t^q$ is a fractional calculus operator is defined as follows:

$$ {}_aD_t^{\gamma}=\begin{cases}\dfrac{d^{\gamma}}{dt^{\gamma}} & \text{if } \gamma>0\\ 1 & \text{if } \gamma=0\\ \displaystyle\int_a^t (d\tau)^{-\gamma} & \text{if } \gamma<0\end{cases} \quad (4)$$

Where γ is a real number representing the fractional order, and a and t are the limits.

One widely recognized form is the Riemann-Liouville model:

$$ {}_aD_t^{\gamma}f(t)=\frac{d^{\gamma}f(t)}{d(t-a)^{\gamma}}=\frac{1}{\Gamma(n-\gamma)}\frac{d^n}{dt^n}\int_0^t\frac{f(\tau)}{(t-\tau)^{\gamma-n+1}}d\tau \quad (5)$$

where n is the lowest integer greater than or equal to γ with Γ() is the gamma function and $n \geq \gamma > n-1$.

Using these principles, these mathematical tools have been effectively applied in control theory, most notably in the development of the FOPID controller.

The FOPID is a versatile controller used for control purposes [14]. It is characterized by five parameters: the proportional gain (K_p), the integrating gain (K_i), the derivative gain (K_d), the integrating order (λ) and the derivative order (μ). The block diagram for a $PI^{\lambda}D^{\mu}$ controller is shown in Figure 1 its transfer function is presented as:

$$H(s)=K_p+\frac{K_i}{s^{\lambda}}+K_ds^{\mu} \quad (6)$$

Approximation and numerical methods have been extensively used because most fractional-order differential equations do not have exact analytic solutions. Therefore, numerical approaches have been developed to solve them.

The approximation for $0<\gamma<1$, where γ represents the fractional order parameter, is given as:

$$s^{\gamma}\approx K\prod_{l=-N}^{N}\frac{s+\mathrm{h}_z}{s+\mathrm{h}_p} \quad (7)$$

where:

$$\mathrm{h}_z=f_l\left(\frac{f_\mathrm{h}}{f_l}\right)^{\frac{l+N+\frac{1}{2}(1-\gamma)}{2N+1}} \quad (7.1)$$

$$\mathrm{h}_p=f_l\left(\frac{f_\mathrm{h}}{f_l}\right)^{\frac{l+N+\frac{1}{2}(1+\gamma)}{2N+1}} \quad (7.2)$$

$$K=f_\mathrm{h}^{\gamma} \quad (7.3)$$

The approximation is applicable within the specified frequency range $f=[f_l,f_\mathrm{h}]$, where f_h is the specified high-frequency limit, f_l is the low-frequency limit and N is the number of poles and zeros. The constant K denotes the gain, and l is an index variable. For fractional order where $\alpha\geq 1$, we have:

$$s^{\alpha}=s^ns^{\gamma} \quad (7.4)$$

where $n=\alpha-\gamma$ denotes the integer part of α and s^{γ} is obtained by equation 7.

The number of poles and zeros is predetermined; lower values of N yield simpler approximations, however, this comes at the cost of introducing ripples in both the gain and phase responses.

To employ the fractional-order controller, the MATLAB-based FOMCON (Fractional-Order Modelling and Control) v1.50.4 toolbox is used. FOMCON is a comprehensive software package designed for the modelling, analysis, identification, and control of fractional-order dynamical systems. The toolbox provides dedicated modules for fractional-order system analysis, controller design, and system identification thereby facilitating the development and evaluation of fractional-order control strategies [34,35]. In this work, we used "Fractional PID Controller" Simulink block only.

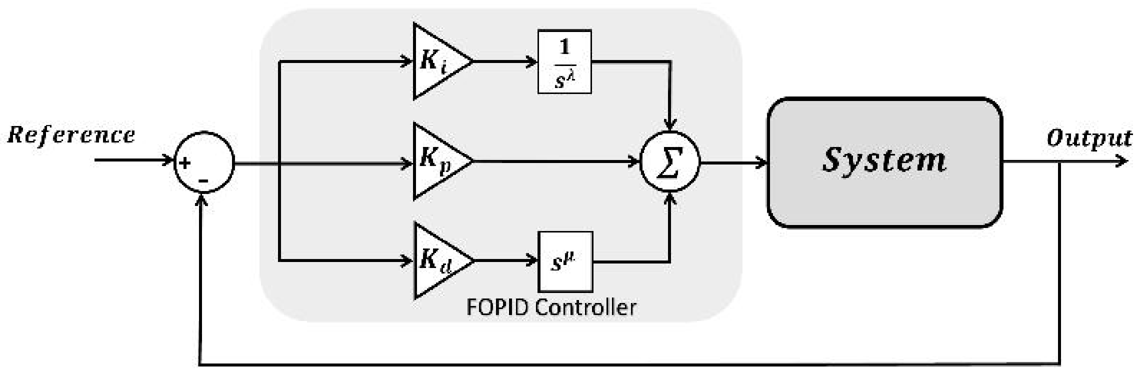

Figure 1. FOPID controller block diagram.

4. Feedback Control System

The DFIG wind energy system integrates various components, prominently featuring the RSC and GSC controllers. The RSC efficiently controls both active and reactive power, while the GSC monitors and maintains the DC-link voltage and produces independent reactive power that is fed into the grid. Assuming the electrical network is stable, the stator flux remains unchanged. In medium to high-power DFIGs, the stator resistance is so small that it can be neglected, simplifying the equations that regulate stator voltages and fluxes as:

$$\begin{cases} V_{ds}=0 \\ V_{qs}=V_s=\omega_s \Psi_{ds} \end{cases} \tag{8}$$

$$\begin{cases} \Psi_{ds}=L_m i_{dr}+L_s i_{ds} \\ \Psi_{qs}=L_m i_{qr}+L_r i_{qs}=0 \end{cases} \tag{9}$$

The active and reactive stator powers and rotor voltages are provided, respectively, as:

$$\begin{cases} P_s=-\frac{3}{2}\frac{L_m}{L_s}V_s i_{rq} \\ Q_s=\frac{3}{2}\left(\frac{V_s^2}{\omega_s L_s}-\frac{L_m}{L_s}V_s i_{rd}\right) \end{cases} \tag{10}$$

$$\begin{cases} V_{dr}=R_r i_{dr}+\sigma L_r \frac{di_{dr}}{dt}-\sigma\omega_{\text{slip}} L_r i_{qr} \\ V_{qr}=R_r i_{qr}+\sigma L_r \frac{di_{qr}}{dt}+\sigma\omega_{\text{slip}} L_r i_{dr}+\frac{L_m}{L_s}\omega_{\text{slip}} \Psi_{ds} \end{cases} \tag{11}$$

where $\sigma=L_r-L_m^2/L_s$ and $\omega_{slip}=\omega_s-\omega_r$ such that ω_r is the angular rotor speed.

As observed from Equation 11, the control at the RSC involves adjusting the rotor currents, which allows for the regulation of the active and reactive power of the DFIG stator.

The compensation term and the PI controller are integrated into the control law as follows:

$$\begin{aligned} v_{\text{dr}}^{*}&=K_{p1}e_d+K_{i1}\int e_d d\tau-\left(\sigma\omega_{slip}L_r i_{qr}\right) \\ v_{\text{qr}}^{*}&=K_{p2}e_q+K_{i2}\int e_q d\tau+\left(\sigma\omega_{slip}L_r i_{dr}+\frac{L_m}{L_s}\omega_{slip}\Psi_{ds}\right) \end{aligned} \tag{12}$$

where $e_q=i_{qrref}-i_{qr}$ and $e_d=i_{drref}-i_{dr}$ are the errors for the d–q rotor currents, K_p and K_i are the proportional and integral gains.

The dc-link, between the two converters, is regulated by the dynamics represented by [36]:

$$\frac{dV_c}{dt}=\frac{v_d}{CV_{dc}}i_d-\frac{1}{C}I_r \tag{13}$$

where V_{dc} is the dc-link voltage, v_d is the d-component of the grid converter voltage, I_r is the current from RSC and C is the capacitance of the dc-link capacitor. Thus, the control law is:

$$i_{dref}=K_{p3}e_v+K_{i3}\int e_v d\tau \tag{14}$$

where $e_v = V_{dcref} - V_{dc}$ is the voltage tracking error.

Figure 2 displays the block diagram of the offline optimization and control strategy.

For simplicity, the formulation given in equation 4 is adopted. Accordingly, equations 12 and 14 can be expressed in a generalized form representing the FOPI controller as follows:

$$\begin{cases} v_{\text{dr}}^{*}=K_{p1}e_d+K_{i1}D_t^{\lambda_1}(e_d)-\left(\sigma\omega_{slip}L_r i_{qr}\right) \\ v_{\text{qr}}^{*}=K_{p2}e_q+K_{i2}D_t^{\lambda_2}\left(e_q\right)+\left(\sigma\omega_{slip}L_r i_{dr}+\frac{L_m}{L_s}\omega_{slip}\Psi_{ds}\right) \end{cases} \tag{15}$$

$$i_{dref}=K_{p3}e_v+K_{i3}D_t^{\lambda_3}(e_v) \tag{16}$$

Where λ_i presents the fractional order.

5. Statement of the Minimization Problem

The purpose of the optimization is to decrease the error of the dc-link voltage V_{dc}, the rotor current on the d-axis i_{rd}, and the rotor current on the q-axis i_{rq}, by optimizing the PI control parameters $K_{p1}, K_{i1}, K_{p2}, K_{i2}, K_{p3}, K_{i3}$ and secondly, optimizing the fractional coefficient $\lambda_1, \lambda_2, \lambda_3$ with four different algorithms:

Particle Swarm Optimization (PSO), Grey Wolf Optimization (GWO), Equilibrium Optimizer (EO), and Harris Hawk Optimization (HHO).

5.1 Particle Swarm Optimization

PSO is a stochastic optimization technique developed by Dr. Eberhart and Dr. Kennedy [37], and it is one the most widely used algorithms in many optimization engineering problems. It is inspired by the social behaviour and swarm intelligence of animals in nature, namely bird flocking and fish schooling. The algorithm is based on the natural process of group communication to share individual knowledge when a group of birds or insects search food or migrate and so forth in a searching space, although all birds or insects do not know where the best position is. But from the nature of social behaviour, if any member can find a desirable path to go, the rest of the members will follow quickly

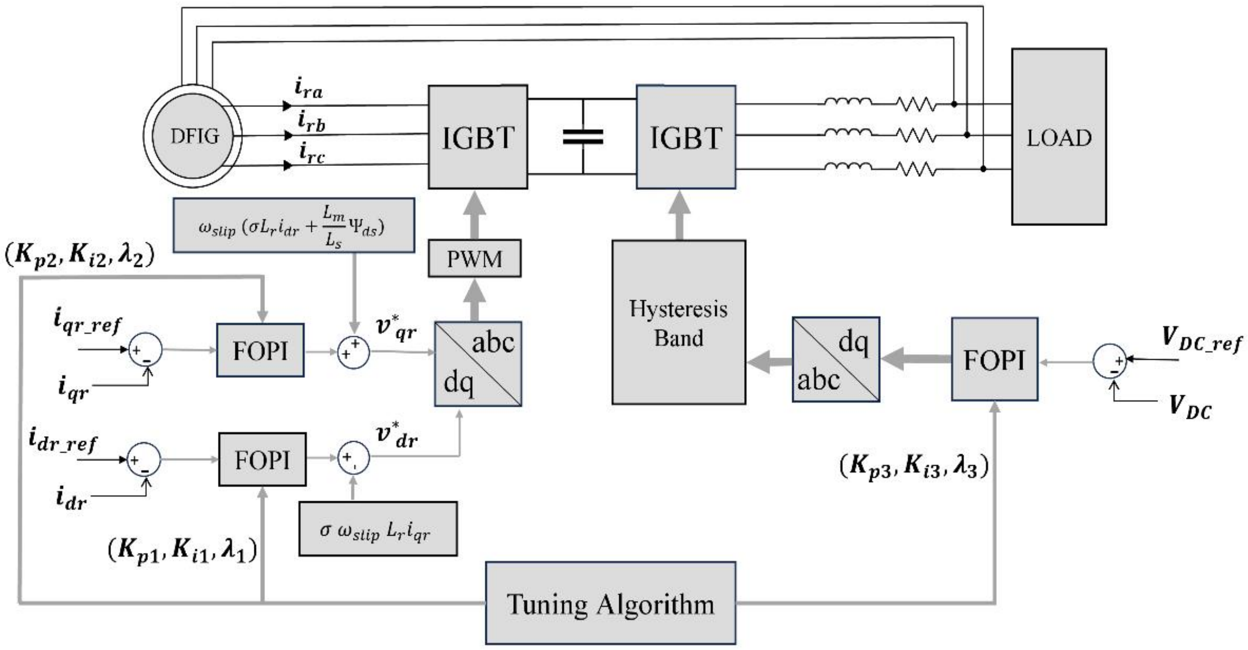

Figure 2. RSC and GSC control systems for the DFIG system.

5.2 Harris Hawks Optimization

HHO is a well-known swarm-based optimization algorithm that has numerous active and time-varying exploration and exploitation phases. This method was first published in 2019 [38], and it has attracted increasing attention among researchers since then due to its flexible structure, excellent performance, and high-quality outcomes. The HHO method's basic reasoning is based on the natural cooperative behaviour and chasing tactics of Harris' hawks known as "surprise pounce".

5.3 Equilibrium Optimizer

The EO is a recent population-based metaheuristic optimization algorithm proposed by Faramarzi et al. [39], inspired by the dynamic mass balance equation used to describe concentration changes in control volume systems. EO models the optimization process based on the concept of achieving an equilibrium state, where particles gradually move toward optimal solutions while maintaining a balance between exploration and exploitation capabilities.

5.4 Proposed Algorithm: Grey Wolf Optimization

This algorithm is inspired by the social dynamics exhibited by the grey wolf, which engages in the pursuit of significant prey collectively and depends on the collaborative efforts of its pack members [40]. There are two interesting features to this behaviour: hunting strategy and social structure. With a complex social structure, the grey wolf is a significantly sociable species. "Dominance hierarchies" denotes a structured ranking system in which wolves are ordered as alphas, betas, deltas, and omegas according to their strength and authority. In addition to their social hierarchy, grey wolves exercise a distinct and strategic hunting approach in the following order:

1. Chasing the prey.
2. Following the prey until it halts its movement.
3. Attack the prey when it is exhausted.

Applying the previously described strategies, each hunting step will be modelled with a mathematical equation.

5.4.1 Exploration And Exploitation

The two main parameters that control the ratio between exploration and exploitation phases are the parameters R and α. With α being decreased throughout the optimization process (since $\vec{\beta}$ is linearly reduced over $[0,2]$), fifty percent of the iterations are for exploration while the remaining for exploitation ($|\alpha|<1$).

5.4.2 Encircling the Prey

The encircling strategy is expressed with following equations:

$$\vec{\delta}=\left\|\vec{R}\cdot\overrightarrow{P_{\text{prey}}}(t)-\vec{P}(t)\right\| \quad (17)$$

$$\vec{P}(t+1)=\overrightarrow{P_{\text{prey}}}(t)-\vec{\alpha}\cdot\vec{\delta} \quad (18)$$

Where: $\overrightarrow{P_{prey}}$ is the vector's position of the prey, $\vec{P}$ is the individual position vector, $\vec{\alpha}$ and $\vec{R}$ are coefficient vectors, and t indicates the current iteration. The vectors $\vec{\alpha}$ and $\vec{R}$ are calculated as follows:

$$\vec{\alpha}=2\vec{\beta}\cdot\vec{x_1}-\vec{\beta} \quad (19)$$

$$\vec{R}=2\cdot\ \vec{x_2} \quad (20)$$

Where $\vec{x_1}$ and $\vec{x_2}$ are random vectors in the interval [0,1]. Whereas $\vec{\beta}$ is a linearly decreased parameter from 2 to 0.

5.4.3 Hunting

During the hunting phase, the GWO assumes alpha and beta agents have stronger insight regarding probable prey locations. These agents then use the following equations to govern the search process:

$$\vec{\delta}_{\text{alpha}}=\left\|\vec{R_1}\cdot\ \overrightarrow{P_{\text{alpha}}}-\vec{P}\right\| \quad (21)$$

$$\vec{\delta}_{\text{beta}}=\left\|\vec{R_2}\cdot\ \overrightarrow{P_{\text{beta}}}-\vec{P}\right\| \quad (22)$$

$$\vec{\delta}_{\text{delta}}=\left\|\vec{R_3}\cdot\ \overrightarrow{P_{\text{delta}}}-\vec{P}\right\| \quad (23)$$

Where $\vec{R_1}$, $\vec{R_2}$, $\vec{R_3}$ are randomly generated vectors, and $\vec{P}$ represents the position vector. $\overrightarrow{P_{\text{alpha}}}$, $\overrightarrow{P_{\text{beta}}}$ and $\overrightarrow{P_{\text{delta}}}$ are the position vector of alpha, beta, and delta respectively.

Equations 21, 22, and 23 determine the length of actual individual and the individual alpha, beta, and delta. Therefore, the final location of the present person is determined by:

$$\vec{P_1}=\overrightarrow{P_{\text{alpha}}}-\vec{\alpha_1}\cdot\ \left(\overrightarrow{\delta_{\text{alpha}}}\right) \quad (24)$$

$$\vec{P_2}=\overrightarrow{P_{\text{beta}}}-\vec{\alpha_2}\cdot\ \left(\overrightarrow{\delta_{\text{beta}}}\right) \quad (25)$$

$$\vec{P_3}=\overrightarrow{P_{\text{delta}}}-\vec{\alpha_3}\cdot\ \left(\overrightarrow{\delta_{\text{delta}}}\right) \quad (26)$$

$$\vec{P}(t+1)=\frac{\vec{P_1}+\vec{P_2}+\vec{P_3}}{3} \quad (27)$$

Where $\vec{\alpha_1}$, $\vec{\alpha_2}$, *and* $\vec{\alpha_3}$ are randomly generated vectors.

5.5 Mathematical Formulation of the Optimization

The variables which were altered repeatedly throughout the optimization process to generate optimal responses for the active/reactive power and DC-link loops are specified as the proportional, integral, and lambda gains:

$$Y=\left[K_{p1},K_{i1},\lambda_1,K_{p2},K_{i2},\lambda_2,K_{p3},K_{i3},\lambda_3\right]$$

These gains are restricted in a specific bounded space such as:

$$\underline{Y}\leq Y\leq\bar{Y}\ i\in(1,2,3)$$

where $\underline{Y}$, $\bar{Y}$ are the lower and the upper bound, respectively.

In this work, an Integral Absolute Error (IAE) was used as a performance index for the objective function, the cost function was expressed as:

$$J_{IAE}(Y)=c_{\text{d}}\int_0^T |e_{\text{d}}(Y,t)|dt+c_{\text{q}}\int_0^T |e_{\text{q}}(Y,t)|dt+c_v\int_0^T |e_v(Y,t)|dt \quad (28)$$

Where c_d, c_q *and* c_v are the weighting factors.

The tuning procedure of the FOPI controller is summarized in Algorithm 1.

Algorithm 1: Two-Stage Metaheuristic Tuning of the FOPI Controller

---

- Initialize model and set parameters: DFIG parameters (Table 4), $fl = 10^{-4}$, $fh = 10^{4}$, $N = 4$
- Define the parameter vector $Y = [K_{p1}, K_{i1}, \lambda_1, K_{p2}, K_{i2}, \lambda_2, K_{p3}, K_{i3}, \lambda_3]$
- Set boundaries [0,20] for K_p, K_i and [0.5,1.5] for λ ; Set $N_A = 20,\ N_i = 50$

for *(each algorithm: GWO, PSO, EO, HHO)* **do**

  Stage 1: Optimize PI

  Initialize population: $\left\{Z_k^{(1)}\right\}_{k=1}^{N_A} : Z_k^{(1)} = \left(K_{p1}, K_{i1}, K_{p2}, K_{i2}, K_{p3}, K_{i3}\right)_k$

  Launch sim() and evaluate $J_{IAE}\left(Z_k^{(1)}\right)$ for each agent (Eq(28))

  $t \leftarrow 0$

  while ($t < N_i$) **do**

    for $k = 1$ to N_A **do**

      Update agent $Z_k^{(1)}$ according to the algorithm's equations

      Launch $sim()$

      Evaluate $J_{IAE}\left(Z_k^{(1)}\right)$

    Update $Z_{\text{best}}^{(1)}$: $Z_{\text{best}}^{(1)}(t+1) = \arg\min\left\{J_{IAE}\left(Z_{\text{best}}^{(1)}(t)\right), J_{IAE}\left(Z_k^{(1)}(t+1)\right) \forall k\right\}$

    Increment $t : t \leftarrow t + 1$

  Return the best PI gains $K_{p1}^*, K_{i1}^*, K_{p2}^*, K_{i2}^*, K_{p3}^*, K_{i3}^* \leftarrow Z_{\text{best}}^{(1)}$

  Stage 2: Optimize the fractional order

  Fix $K_{p1,2,3} = K_{p1,2,3}^*$ and $K_{i1,2,3} = K_{i1,2,3}^*$ from Stage 1

  Initialize population $\left\{Z_k^{(2)}\right\}_{k=1}^{N_A} : Z_k^{(2)} = (\lambda_1, \lambda_2, \lambda_3)_k$

  Launch $sim()$ and evaluate $J_{IAE}\left(Z_k^{(2)}\right)$ for each agent (Eq(28))

  $t \leftarrow 0$

  while ($t < N_i$) **do**

    for $k = 1$ to N_A **do**

      Update agent $Z_k^{(2)}$ according to the algorithm's equations

      Launch $sim()$

      Evaluate $J_{IAE}\left(Z_k^{(2)}\right)$

    Update $Z_{\text{best}}^{(2)}$: $Z_{\text{best}}^{(2)}(t+1) = \arg\min\left\{J_{IAE}\left(Z_{\text{best}}^{(2)}(t)\right), J_{IAE}\left(Z_k^{(2)}(t+1)\right) \forall k\right\}$

    Increment $t : t \leftarrow t + 1$

  Return the best fractional order values $\lambda_1^*, \lambda_2^*, \lambda_3^* \leftarrow Z_{\text{best}}^{(2)}$

  Save best agent $Y_{\text{Algorithm}}^* = [K_{p1}^*, K_{i1}^*, \lambda_1^*, K_{p2}^*, K_{i2}^*, \lambda_2^*, K_{p3}^*, K_{i3}^*, \lambda_3^*]$

- Evaluate and save the dynamic response of the best FOPI controller found by each algorithm.

---

6. Results and Simulation

The primary objective of this study is to tune high-performance PI and FOPI controllers for a DFIG wind turbine system. The design problem is framed as a control optimization challenge. In the proposed approach, optimization algorithms were employed to determine the optimal controller parameters. All optimization processes were executed offline in the MATLAB/Simulink R2024a environment on a computer equipped with an Intel i7-1165G7 processor (2.80 GHz) and 16 GB of RAM.

The integral of the designed FOPI controller was approximated using a fourth-order transfer function (N = 4), and the frequency limits were set at $f_l = 10^{-4}$ and $f_h = 10^4$, where γ is equivalent to λ.

The optimization process used 20 agents (N_A=20) and 50 iterations (N_i=50). The gains of the PI controller varied within the range of 0 to 20, while for the FOPI controller, the gains ranged from 0.5 to 1.5. The number of agents and the upper and lower bounds remained consistent across all optimization algorithms. The weighting factors in equation (28) are all set to one

$$c_d=c_q=c_v=1.$$

The parameters of each algorithm are detailed in Table 1, while the design specifications are summarized in Table 2:

Table 1. Algorithms parameters.

Algorithms	Parameters
GWO [40]	$\beta \in [2, 0]$
PSO [37]	$w \in [2, 0]$ $c1 = 2$ $c2 = 1.5$
HHO [38]	None
EO [39]	$a1 = 2$ $a2 = 1$ $V = 1$ $GP = 0.5$

Table 2. Design specifications.

	K_p	K_i	λ
N_i	50	50	50
N_A	20	20	20
Range	[0, 20]	[0, 20]	[0.5, 1.5]

The corresponding DIFG specifications are provided in Table 4.

6.1 Algorithms Comparison

In this part, the performance of the metaheuristic algorithms is analysed and compared to determine the most effective optimization method. The algorithm achieving the best results is subsequently candidate to carry out a comparative assessment between the conventional PI controller and the optimized FOPI controller. The following graphs represent the step response of the DC-link voltage and the d-q rotor current controllers with different algorithms.

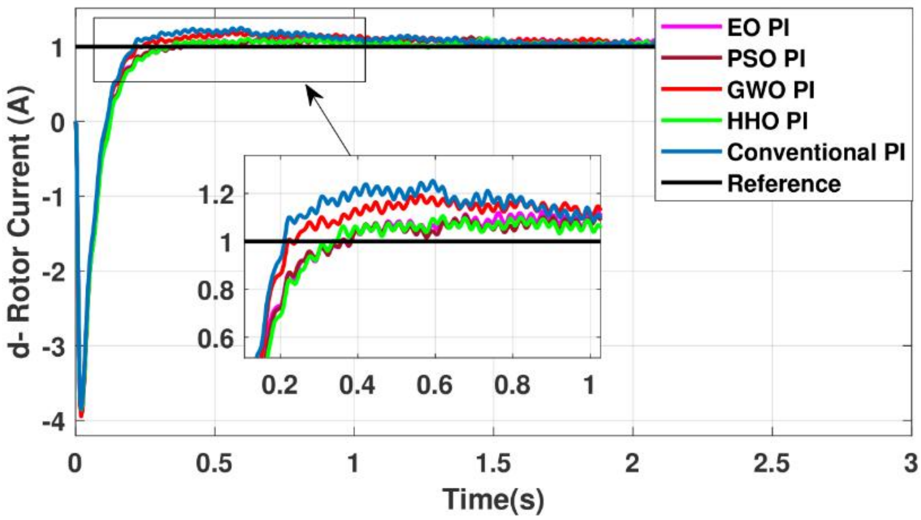

Figure 3. Rotor i_d step response with different algorithms.

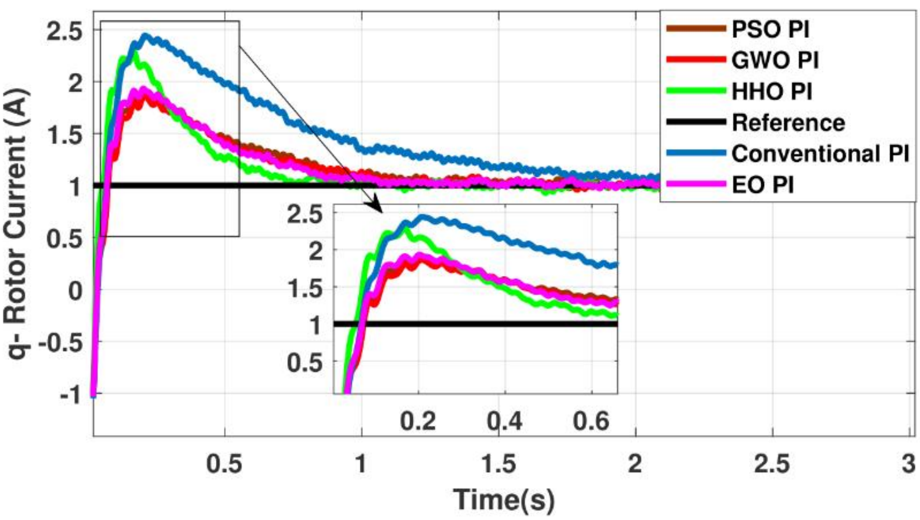

Figure 4. Rotor i_q step response with different algorithms.

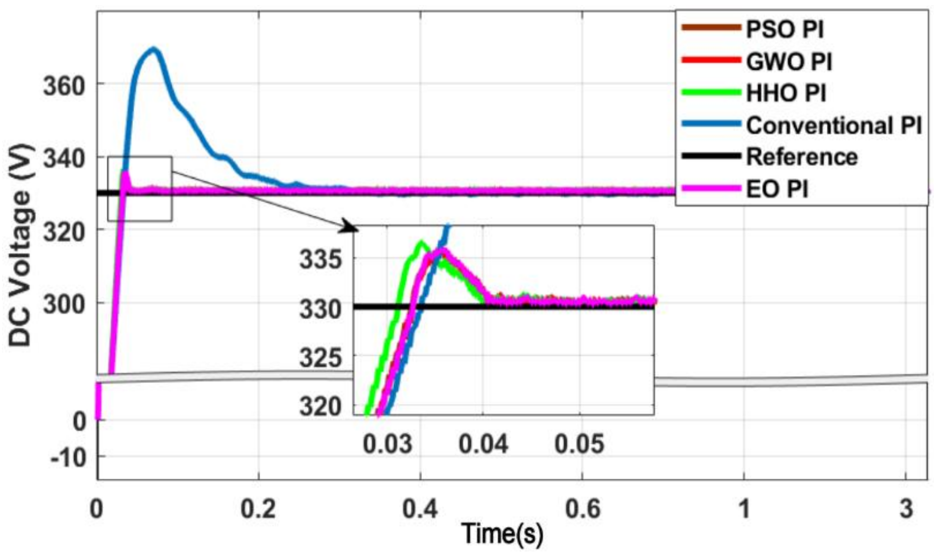

Figure 5. DC-Link step response with different algorithms.

Based on the comparative performance analysis and performance of various algorithms, the results for the terminal closed loop step response in Figure 3, Figure 4, Figure 5 were almost nearly comparable. However, the conventional PI response differs from the others. Table 3 represents the gain values and fitness function for each algorithm for both PI and FOPI. Clearly, for the rotor d-component, the PSO emerged as the top-performing algorithm, while the rotor q-component and DC link voltage, the GWO emerged as the most successful algorithm. These findings provide a concise overview of the comparative performance.

6.2 Controllers Comparison

The data presented in Table 3 indicates that the GWO consistently and effectively performs well. Based on these results, the GWO was selected for conducting the comparative analysis between the conventional PI and FOPI.

Table 3. Optimization results.

		EO	HHO	GWO	PSO	Conventional [32]
I_{RD}	K_p	16.3879	11.1343	18.9924	17.7945	4.5000
	K_i	7.7681	4.2093	18.1964	7.5230	7.5000
	J_{IAE}	2.9971	3.0170	3.0062	**2.9962**	3.0237
	λ	1.4840	0.7623	1.5000	1.2917	
	J_{IAE}	2.9894	2.9932	2.9978	**2.9836**	
I_{RQ}	K_p	6.0133	3.7061	7.2918	6.9800	4.5000
	K_i	19.9620	20.0000	20.0000	18.1736	7.5000
	J_{IAE}	1.6391	1.6876	**1.6177**	1.6381	2.6367
	λ	0.5000	0.5000	0.5000	0.5000	
	J_{IAE}	1.5512	1.6104	**1.5456**	1.5519	
V_{DC}	K_p	19.9506	19.2944	20.0000	17.4070	0.5000
	K_i	0.5000	0.5000	0.5000	0.5000	7.0000
	J_{IAE}	4.1030	4.0971	**4.0930**	4.1288	6.7130
	λ	0.5010	0.5000	0.5000	0.5164	
	J_{IAE}	4.0090	4.0231	**4.0076**	4.0358	

Table 4. DFIG parameters.

DFIG Parameters	*Value*
Power	2 KW
Rated Frequency	60Hz
Pole pairs	2
Mutual inductance	9.45E-02 H
Rotor Resistance	0.68 Ω
Rotor inductance	6.62E-02 H
Stator resistance	0.68 Ω
Stator Inductance	6.62E-02 H

Figure 6, Figure 7, Figure 8 represent the step response of the d-q rotor current and the DC link voltage controllers for the conventional PI and FOPI:

As demonstrated in Figure 7, the Ir-d performance of the FOPI is highlighted, revealing its superior performance in terms of settling time and overshoot compared to the PI controllers. The FOPI controller demonstrated a faster convergence to the reference value, as presented in Table 5. The FOPI controller exhibited a lower overshoot of (0.93 %), outperforming both the GWO PI (2.57 %) and the conventional PI (4.43 %). In addition, the settling time for FOPI was notably shorter at (0.33 s), compared to GWO PI (0.37 s) and conventional PI (1.2 s). The peak values further underscored the efficacy of the FOPI controller, with values of (1.11), as opposed to (1.17) for GWO PI and (1.25) for conventional PI.

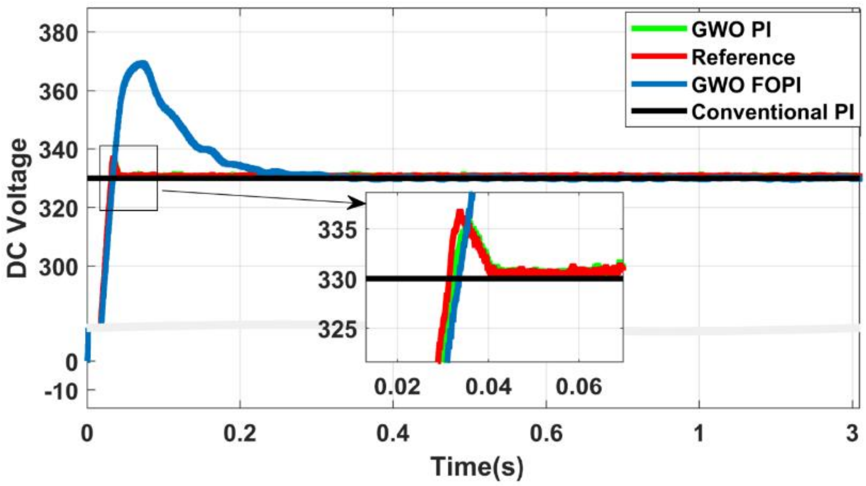

Figure 6. DC-Link PI and FOPI step response.

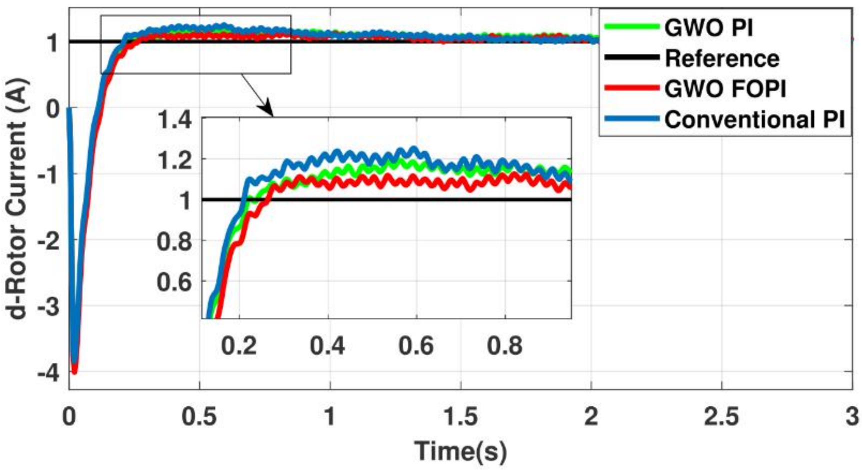

Figure 7. Rotor i_d PI and FOPI step response.

In Figure 8, a distinct contrast is evident between the responses of the controllers, particularly highlighting the superior performance of the FOPI controller compared to the ordinary PI controllers. In particular, the FOPI controller exhibited a considerably lower peak value, settling time, and overshoot. Specifically, the overshoot for FOPI was measured at (21.34 %), significantly outperforming GWO PI (37.88 %) and conventional PI (59.87 %). In addition, the settling time for FOPI was significantly shorter at (0.57 s), in contrast to (1.02 s) and (1.9 s). The peak values further underscored the efficacy of the FOPI controller, with values of (1.48), compared to (1.86) for the GWO PI and (2.44) for the conventional PI.

The response of the DC-Link control, as depicted in Figure 6, highlights the distinct characteristics of the

FOPID controller. Notably, the FOPID controller exhibited a higher overshoot compared to the integer-order controller, indicating a more pronounced deviation from the desired setpoint. However, it should be noted that the FOPID controller demonstrated a shorter settling time (table 5) and lower steady-state error as estimated by the fitness function values in Table 3.

From the Figure 9, Figure 10, Figure 11 the FOPI controller consistently outperformed the conventional PI controller in both transient and steady-state responses for variable step input. The former controller demonstrated faster response times, reduced overshoot, and minimal oscillations, ensuring more accurate and stable tracking of the reference signal. The improved performance was particularly evident in its ability to swiftly and smoothly respond to variable step inputs. This superior handling of dynamic changes indicates that the FOPI controller is more effective.

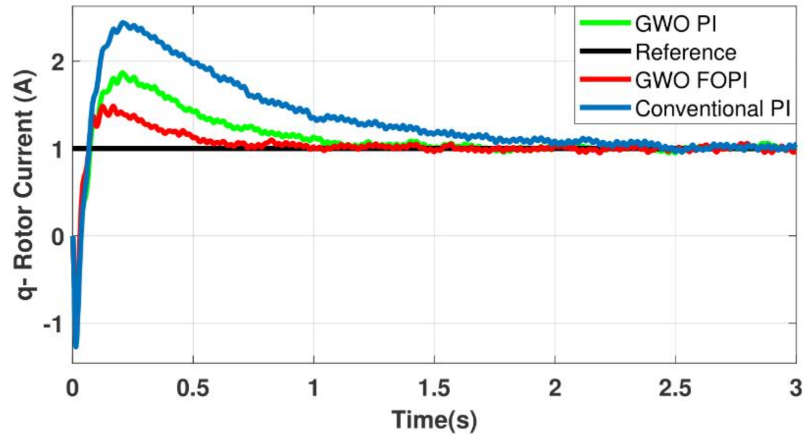

Figure 8. Rotor i_q PI and FOPI step response.

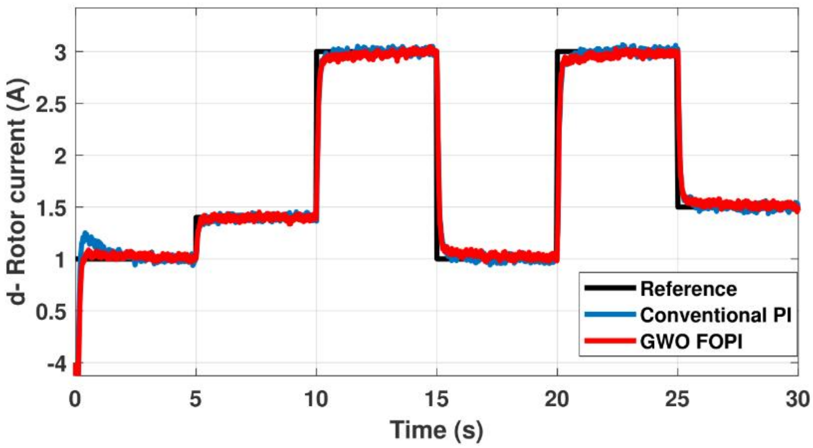

Figure 9. Rotor i_d current response with variable step input.

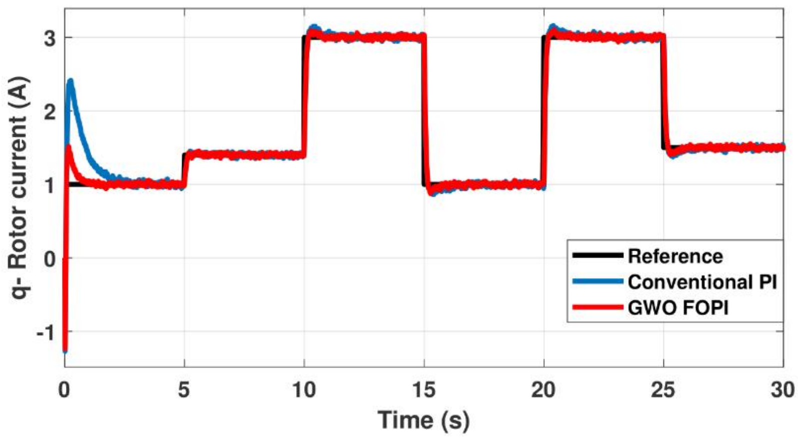

Figure 10. Rotor $i_q$current response with variable step input.

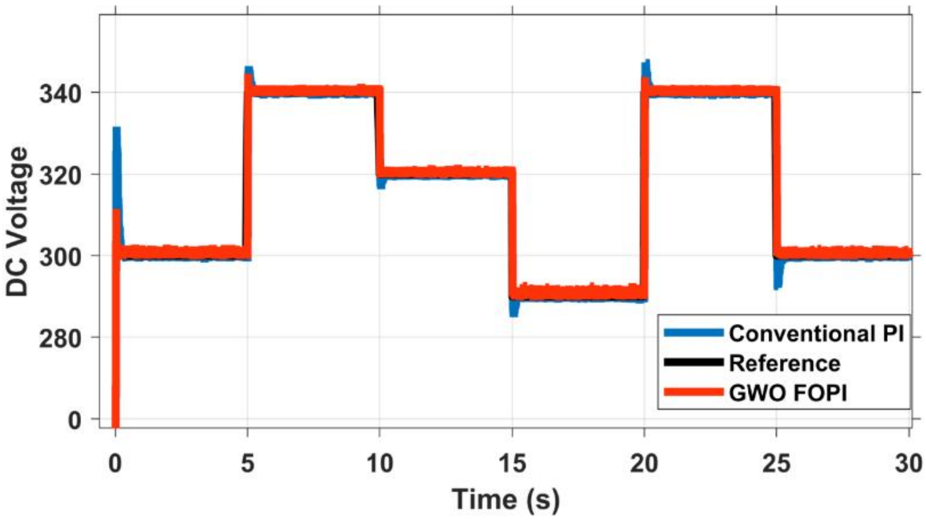

Figure 11. DC-Link response with variable step input.

Although certain controllers showed better dynamic performance (Table 3), this does not always result in a lower cost function due to steady-state error accumulation (Table 5). Therefore, the controller selection should balance transient response and long-term performance.

The two Figure 12 and Figure 13 indicate that the active power response remains nearly identical for both the FOPI and PI controllers. This behaviour is expected, given that Id current in figure 7 shows minimal difference between the two control strategies. The similarity in active power regulation was observed in both the stator and rotor power graphs. However, a significant difference was noted in the reactive power response. The FOPI controller consistently outperformed the conventional PI controller by maintaining a more stable reactive power with lower oscillations and reduced values. In figure 12b, a difference of approximately 20VAR was observed, which was attributed to the distinct behaviour of the Iq current (figure 8) and the instability of rotor reactive power in figure 13b. The advantage of FOPI was even more obvious in the rotor power response, where the PI controller showed excessive oscillations and high variations, while FOPI ensured smoother and more stable reactive power control.

Table 5. Controllers dynamic response.

		EO		HHO		GWO		PSO		Conventional
		PI	FOPI	PI	FOPI	PI	FOPI	PI	FOPI	PI
I_{RD}	Overshoot (%)	1.31	0.36	1.34	0.40	**2.57**	**0.93**	1.05	0.98	**4.43**
	Settling Time (s)	1.07	0.47	0.53	0.47	**0.37**	**0.33**	0.4	0.364	**1.2**
	Peak values	1.11	1.04	1.18	1.11	**1.17**	**1.11**	1.21	1.06	**1.25**
I_{RQ}	Overshoot (%)	40.08	24.37	52.34	27.06	**37.88**	**21.34**	38.19	24.37	**59.87**
	Settling Time (s)	0.67	0.72	1.04	0.97	**1.02**	**0.57**	1.13	0.772	**1.9**
	Peak values	1.93	1.54	1.86	1.48	**1.86**	**1.48**	1.87	1.54	**2.44**
V_{DC}	Overshoot (%)	1.73	1.46	1.66	2.03	**1.68**	**2.03**	1.08	1.53	**11.79**
	Settling Time (s)	0.0415	0.0389	0.0412	0.0405	**0.0422**	**0.0404**	0.0406	0.0379	**0.31**
	Peak values	335.74	334.84	335.49	336.71	**335.57**	**336.74**	335.42	333.59	**369.48**

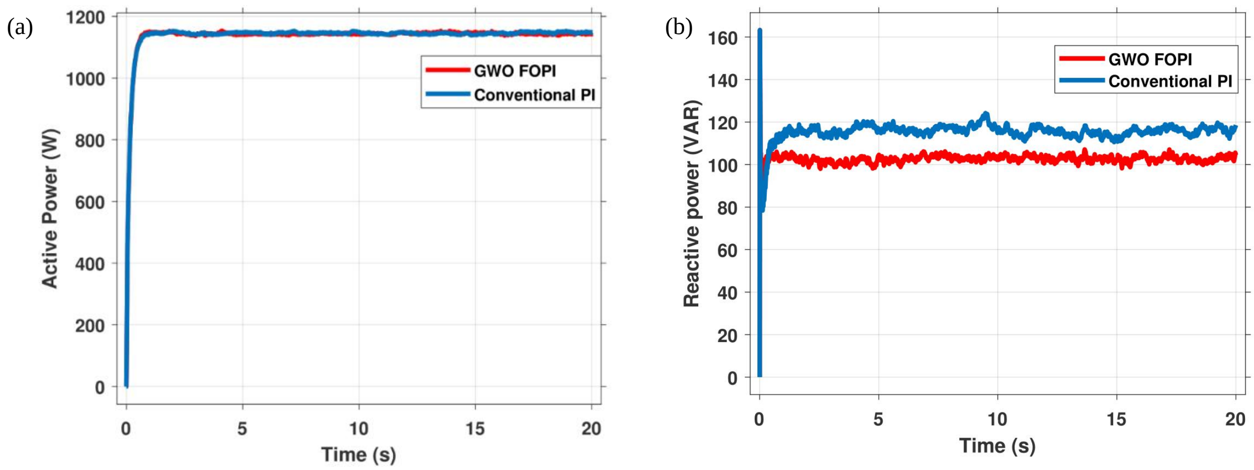

Figure 12. Active and reactive power of the stator: (a) active power; (b) reactive power.

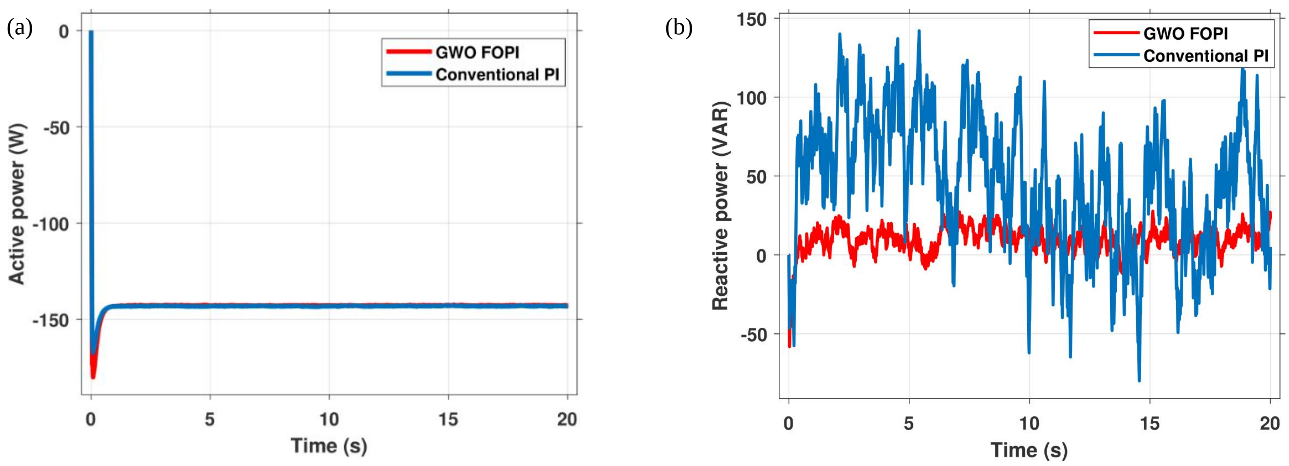

Figure 13. Active and reactive power of the rotor: (a) active power; (b) reactive power.

In summary, across various dynamic responses, the FOPI consistently outperformed PI controllers by achieving lower overshoot, faster settling times, reduced steady-state errors, and enhanced reactive power. These improvements enhanced overall system stability and enable more efficient power extraction.

7. Conclusion

This work explored the use of metaheuristic optimization techniques for the design of a FOPI controller applied to a DFIG-based wind energy conversion system. By combining a two-stage tuning procedure with advanced optimization algorithms, an effective controller configuration was obtained, capable of enhancing the dynamic performance of the system while preserving a relatively simple control structure.

The comparative analysis showed the ability of the optimized FOPI controller to outperform its conventional PI counterpart in terms of transient and steady-state behaviour. The additional degree of freedom introduced by the fractional-order formulation provided greater flexibility in the tuning process, resulting in improved tracking performance and a more satisfactory dynamic response. Moreover, the proposed controller exhibited a favourable impact on reactive power regulation, contributing to smoother system operation and enhanced stability.

The obtained results demonstrate the potential of fractional-order control as a viable alternative to conventional control strategies for DFIG-based wind turbines. More broadly, they highlight the relevance of metaheuristic optimization methods in addressing complex controller tuning problems, where achieving an appropriate balance between performance and implementation simplicity remains a key challenge.

Future work will focus on extending the proposed approach toward fault-tolerant control schemes and investigating its effectiveness under fault conditions and parameter uncertainties

Author Contributions

OAB and KBK contributed to the conceptualization and design of the study. KBK supervised the research. OAB and KBK were responsible for resources, materials, and data collection and/or processing. Data analysis and interpretation were performed by OAB, KBA, and RHE. The original draft of the manuscript was prepared by OAB and RHE. Critical review and revision of the manuscript were carried out by OAB, KBK, KBA, and RHE

Acknowledgements

The authors did not receive any sponsorship to carry out the research reported in the present manuscript.

Conflict of Interest

The authors do not have any type of conflict of interest to declare.

Generative AI Statement

During the preparation of this work, the authors used QuillBot and ChatGPT to rephrase the text and check grammar. After using these tools, the authors reviewed and edited the content and assume full responsibility for the content of the publication.

References

[1] R. Mamat, Erdiwansyah, M.F. Ghazali, S. Rosdi, Syafrizal, Bahagia. Strategic framework for overcoming barriers in renewable energy transition: A multi-dimensional review. Next Energy, 2025, 9, 100414. DOI: 10.1016/j.nxener.2025.100414

[2] T.K. Bashishtha, V.P. Singh, U.K. Yadav, U.K. Sahu. Fractional-order pid controllers and applications: A compre hensive survey. Annual Reviews in Control, 2025, 60, 101013. DOI: 10.1016/j.arcontrol.2025. 101013

[3] H. Rezk, A.G. Olabi, T. Wilberforce, E.T. Sayed. A multi-faceted review of wind turbine optimization techniques: Metaheuristics and related issues. International Journal of Thermofluids, 2025, 26, 101077. DOI: 10.1016/j.ijft.2025.101077

[4] G. Abad, J. López, M. Rodríguez, L. Marroyo, G. Iwanski. Introduction to a wind energy generation system. Doubly Fed Induction Machine: Modeling and Control for Wind Energy Generation Applications, 2011, 1-85. DOI: 10.1002/9781118104965.ch1

[5] H. Bakır, A. Merabet, R.K. Dhar, A.A. Kulaksız. Bacteria foraging optimization algorithm based optimal control for doubly-fed induction generator wind energy system. IET Renewable Power Generation, 2020, 14(11), 1850-1859. DOI: 10.1049/iet-rpg.2020.0172.

[6] M.M. Alhato, S. Bouall`egue. Direct power control optimization for doubly fed induction generator based wind turbine systems. Mathematical and Computational Applications, 2019, 24(3), 77. DOI: 10.3390/mca24030077

[7] R.P. Borase, D.K. Maghade, S.Y. Sondkar, S.N. Pawar. A review of pid control, tuning methods and applications. International Journal of Dynamics and Control, 2021, 9, 818-827. DOI: 10.1007/s40435-020-00665-4

[8] D. Celik, N. Khosravi, M.A. Khan, M. Waseem, H. Ahmed. Advancements in nonlinear pid controllers: A comprehensive review. Computers and Electrical Engineering, 2026, 129, 110775. DOI: 10.1016/ j.compeleceng.2025.110775

[9] A.K. Chen, D. Xie, D.M. Zhang, C.H. Gu, K.Y. Wang. Pi parameter tuning of converters for sub-synchronous interactions existing in grid-connected dfig wind turbines. IEEE Transactions on Power Electronics, 2019, 34(7) 6345-6355. DOI: 10.1109/TPEL.2018.2875350

[10] O.P. Bharti, R.K. Saket, S.K. Nagar. Controller design of dfig based wind turbine by using evolutionary soft computational techniques. Engineering, Technology Applied Science Research, 2017, 7(3), 1732-1736. DOI: 10.48084/etasr.1231

[11] B. Wadawa, Y. Errami, O. Abdellatif, S. Sahnoun, E. Chetouani, M. Aoutoul. Comparative application of the self-adaptive fuzzy-pi controller for a wind energy conversion system connected to the power grid and based on dfig. International Journal of Dynamics and Control, 2022, 10, 2151-2173. DOI: 10.1007/s40435-022-00952-2

[12] B. Wadawa, Y. Errami, A. Obbadi, S. Sahnoun. Pid-fuzzy logic for strategic powers control in a wind energy system using a dfig. 2022 2nd International Conference on Innovative Research in Applied Science, Engineering and Technology (IRASET), 2022, 1-8. DOI: 10.1109/IRASET52964.2022.9737813

[13] A. Aggoune, F. Berrezzek, K. Khelil. Finite-control-set model predictive control (fcs-mpc) and fuzzy self-adaptive pi controller (fsa-pic) for wind turbine system based on dfig. Springer Proceedings in Materials, 2024, 45, 327-338. DOI: 10.1007/978-981-97-1916-7_34

[14] I. Podlubny, L. Dorcak, I. Kostial. On fractional derivatives, fractional-order dynamic systems and piλdμ con trollers. Proceedings of the 36th IEEE Conference on Decision and Control, 1997, 5, 4985-4990. DOI: 10.1109/CDC.1997.649841

[15] A. Asgharnia, R. Shahnazi, A. Jamali. Performance and robustness of optimal fractional fuzzy pid controllers for pitch control of a wind turbine using chaotic optimization algorithms. ISA Transactions, 2018, 79, 127-44. DOI: 10.1016/j.isatra.2018.04.016

[16] P.H. Li, L.Y. Xiong, Z.Q. Wang, M.L. Ma, J. Wang. Fractional-order sliding mode control for damping of subsynchronous control interaction in dfig-based wind farms. Wind Energy, 2019, 23(3), 749-762. DOI: 10.1002/we.2455

[17] B. Yang, T. Yu, H. Shu, Y.M. Han, P.L. Cao, L. Jiang. Adaptive fractional-order pid control of pmsg-based wind energy conversion system for mppt using linear observers. International Transactions on Electrical Energy Systems, 2018, 29 (1), e2697. DOI: 10.1002/etep.2697

[18] H. Benbouhenni, N. Bizon, I. Colak, P. Thounthong, N. Takorabet. Application of fractional-order pi controllers and neuro-fuzzy pwm technique to multi-rotor wind turbine systems. Electronics, 2022, 11(9) 1340. DOI: 10.3390/ electronics11091340

[19] S. Alyafeai, K.B. Gaufan, N.M. Alyazidi. Comparative study of pid and fopid controllers tuned by metaheuristic algorithms for microgrid systems. Transportation Research Procedia, 2026, 96, 316-323. DOI: 10.1016/j.trpro.2026.03.041

[20] C. Wang, H. Zhang, D.L. Wen, M.Q. Shen, L.W. Li, Z.H. Zhang, Novel passivity and dissipativity criteria for discrete time fractional generalized delayed cohen-grossberg neural networks. Communications in Nonlinear Science and Numerical Simulation, 2024, 133, 107960. DOI: 10.1016/j.cnsns.2024.107960

[21] M.Q. Shen, C. Wang, Q.G. Wang, Y.H. Sun, G.D. Zong. Synchronization of fractional reaction-diffusion complex networks with unknown couplings. IEEE Transactions on Network Science and Engineering, 2024, 11(5), 4503-4512. DOI: 10.1109/TNSE.2024.3432997

[22] M.Q. Shen, C. Wang, Q.G. Wang, H.C. Yan, G.D. Zong, Z.H. Zhu. Fault-tolerant synchronization control of switched complex networks by a proportional-integral intermediate observer approach. IEEE Transactions on Cybernetics, 2025, 55(10), 4689-4698. DOI: 10.1109/TCYB.2025.3591393

[23] I. Paducel, C.O. Safirescu, E.-H. Dulf. Fractional order controller design for wind turbines. Applied Sciences, 2022, 12(17), 8400. DOI: 10.3390/app12178400
[24] M.I. Mossad. Application of dpc to improve the integration of dfig into wind energy conversion systems using fopi controller. Wind Engineering, 2025, 49(1), 129-141. DOI: 10.1177/0309524X241256956
[25] S. Noureddine, S. Morsli, A. Tayeb. Optimized fuzzy fractional pi-based mppt controllers for a variable-speed wind turbine. Wind Engineering, 2022, 46(6), 1721-1734. DOI: 10.1177/0309524X221102794
[26] M. Vijayalaxmi, P. Thevamudhan. Enhancing power quality in doubly fed induction generator-based wind energy conversion systems using fopid controller. Journal of Circuits, Systems and Computers, 2026, 35(13), 2650060. DOI: 10.1142/S021812662650060X
[27] S. Yamparala, L. Lakshminarasimman, G. Sambasiva Rao. Optimal design of fopid controller for dfig based wind energy conversion system using grey-wolf optimization algorithm. International Journal of Renewable Energy Research, 2022, 12(4), 2110-2119.
[28] M. Dahane, A. Benali, H. Tedjini, A. Benhammou, M.A. Hartani, H. Rezk. Optimized double-stage fractional order controllers for dfig-based wind energy systems: A comparative study. Results in Engineering, 2025, 25, 104584. DOI: 10.1016/j.rineng.2025.104584
[29] N. Bouderres, D. Kerdoun, A. Djellad, S. Chiheb, A. Dekhane. Optimization of fractional order pi controller by pso algorithm applied to a grid-connected photovoltaic system. Journal Europ´een des Syst`emes Automatis´es, 2022, 55(4), 427-438. DOI: 10.18280/jesa.550401
[30] H. Benbouhenni, I. Colak, Z.M.S. Elbarbary, S.M. Irshad. Reducing power ripple for multi-rotor wind energy systems using fopdpi controllers. Scientific Reports, 2025, 15, 12524. DOI: 10.1038/s41598-025-96625-z
[31] Z. Bingul, O. Karahan. Comparison of pid and fopid controllers tuned by pso and abc algorithms for unstable and integrating systems with time delay. Optimal Control Applications and Methods, 2018, 39(4), 1431-1450. DOI: 10.1002/oca.2419
[32] A.A. Tanvir, A. Merabet, R. Beguenane. Real-time control of active and reactive power for doubly fed induction gen erator (dfig)-based wind energy conversion system. Energies, 2015, 8(9), 10389-10408. DOI: 10.3390/en80910389
[33] O. Barambones, J.A. Cortajarena, P. Alkorta, J.M.G. De Durana. A real-time sliding mode control for a wind energy system based on a doubly fed induction generator. Energies, 2014, 7(10), 6412-6433. DOI: 10.3390/ en7106412
[34] A. Tepljakov, E. Petlenkov, J. Belikov. Fomcon: A matlab toolbox for fractional-order system identification and control. International Journal of Microelectronics and Computer Science, 2011, 2(2), 51-62.
[35] A. Tepljakov. Fomcon: Fractional-order modeling and control toolbox. Springer, Cham, 2017. 107-129.
[36] A. Merabet, K.T. Ahmed, R. Beguenane, H. Ibrahim. Feedback linearization control with sliding mode disturbance compensator for pmsg based wind energy conversion system. 2015 IEEE 28th Canadian Conference on Electrical and Computer Engineering (CCECE), 2015, 943-947. DOI: 10.1109/CCECE.2015.7129402
[37] J. Kennedy, R. Eberhart. Particle swarm optimization. Proceedings of ICNN'95- International Conference on Neural Networks, 1995, 4, 1942-1948. DOI: 10.1109/ICNN.1995.488968
[38] A.A. Heidari, S. Mirjalili, H. Faris, I. Aljarah, M. Mafarja, H. Chen. Harris hawks optimization: Algorithm and applications. Future Generation Computer Systems, 2019, 97, 849-872. DOI: 10.1016/j.future. 2019.02.028
[39] A. Faramarzi, M. Heidarinejad, B. Stephens, S. Mirjalili. Equilibrium optimizer: A novel optimization algorithm. Knowledge-Based Systems, 2020, 191, 105190. DOI: 10.1016/j.knosys.2019.105190
[40] S. Mirjalili, S.M. Mirjalili, A. Lewis. Grey wolf optimizer. Advances in Engineering Software, 2014, 69, 46-61. DOI: 10.1016/j.advengsoft.2013.12.007